

Title	Micromechanical fiber optic switches for optical networks
Authors	Riza, Nabeel A.;Polla, Dennis L.
Publication date	1993-03-02
Original Citation	Riza, N. A. and Polla, D. L. [1993] 'Micromechanical fiber optic switches for optical networks", Proc. SPIE 1793, Integrated Optics and Microstructures, Fibers '92, 1992, Boston, MA, United States, 2 March 1993. doi: 10.1117/12.141209
Type of publication	Conference item
Link to publisher's version	10.1117/12.141209
Rights	© 1993 Society of Photo-Optical Instrumentation Engineers (SPIE). One print or electronic copy may be made for personal use only. Systematic reproduction and distribution, duplication of any material in this paper for a fee or for commercial purposes, or modification of the content of the paper are prohibited.
Download date	2024-04-20 09:31:12
Item downloaded from	<a href="https://hdl.handle.net/10468/10134">https://hdl.handle.net/10468/10134</a>

# PROCEEDINGS OF SPIE

[SPIDigitalLibrary.org/conference-proceedings-of-spie](https://SPIDigitalLibrary.org/conference-proceedings-of-spie)

## Micromechanical fiber optic switches for optical networks

Riza, Nabeel, Polla, Dennis

Nabeel A. Riza, Dennis L. Polla, "Micromechanical fiber optic switches for optical networks," Proc. SPIE 1793, Integrated Optics and Microstructures, (2 March 1993); doi: 10.1117/12.141209

**SPIE.**

Event: Fibers '92, 1992, Boston, MA, United States

## Micromechanical fiber-optic switches for optical networks

Nabeel A. Riza

General Electric Corporate Research and Development Center,  
P. O. Box 8, KWB 617, Schenectady, N. Y. 12301

and

Dennis L. Polla

Dept. of Electrical Engineering  
University of Minnesota  
Minneapolis, MN 55455

### **ABSTRACT**

Piezoelectric thin film actuator-based fiber-optic switches are introduced as low loss, high interchannel optical isolation 1 X 2 and 2 X 2 fiber-optic switches. A macroscale PZT actuator is built and tested. Preliminary results from a microscale actuator are given. Optical switch configurations and fabrication procedures are highlighted.

### **2. INTRODUCTION**

At present, there is a need for low cost, low loss, high channel-isolation, fiber-optic switches for use in next-generation high performance optical networks in phased array antenna control, aircraft engine sensor networks, and communication systems. For aircraft engine and other high temperature environments, the switch must withstand high temperature and dirty settings. Various technologies have been employed in making fiber-optic switches; prominent among these are the lithium niobate-based switches and liquid crystal switches. So far, lithium niobate-based 2 X 2 fiber-optic switches are expensive, lossy (e.g., 5 dB optical insertion loss per switch), and have moderately good (e.g., 20 dB) channel isolation. Thus, for applications such as optically controlled phased arrays that require thousands of switches arranged in cascade configurations, the lithium niobate optical switches are not a practical and economical solution. Recently, nematic liquid crystal switches have shown relatively high (e.g., 36 dB optical ) on/off ratios along with low (<1 dB) optical insertion losses [1]. Although liquid crystals are a promising optical switch technology, they cannot be operated in high temperature environments such as aircraft engines.

Recently, researchers at NTT Japan and Texas Instruments (TI) have suggested the use of micromechanics for fiber-optic switching using electrostatic forces [2-4]. These micromechanical optical switches use simple parallel plate actuator-type geometries to generate translational forces that effect the optical propagation of light to implement the optical routing. In this paper, we introduce the use of micromachined piezoelectric thin-film microactuators for fiber-optic switching. The use of piezoelectric thin films for microactuation has certain advantages that include the ability to use surface micromachining to build complex mechanical structures that provide stable translational control at moderate voltage levels, in addition to having features like large force generation capability that can lead to faster responses, and compatibility with silicon and gallium arsenide electronics.

Thus, it is through the merging of three technologies, namely, fiber-optics, microoptics, and silicon-based micromachining using piezoelectric thin films, that this paper explores the possibility of a microdynamical fiber-optic switch, that through the unique features of a silicon-based piezo-electric microactuators, single-mode fibers, and micro-optics, will provide the features desired for commercial fiber-optic switching applications.

### **3. OPTICAL SWITCH REQUIREMENTS**

There are two basic sizes that are appropriate for making these switches using thin-film microactuators. They are the 1 X 2 configuration (see Fig.1) and the 2 X 2 configuration (see Fig.2). Note that two 1 X 2 switches can be combined with two standard passive fiber-optic couplers to give a 2 X 2 configuration, as shown in Fig.1. The goal is to make a small 1 X2 or 2 X 2 switch that has very high optical interchannel isolation (> 50 dB), and can be produced at low cost. The key motivation for these switch requirements arises from the wide bandwidth phased array radar application. In particular, switched time delays are required in controlling wide bandwidth phased array antennas.

Fig.3 shows a typical serial digitally switched delay line structure that is required for controlling an antenna element or subarray. Optical delay lines appear promising as wide instantaneous bandwidth (e.g., 2 GHz), long optical time delays (e.g., 10 ns) can be achieved with extremely low optical propagation losses and low EMI effects as compared to electrical/rf delay lines. In particular, fiber-based optical delay lines could form robust, compact, long time delay units. The key hurdle in achieving this fiber delay unit is a low loss ( $< 1$  dB), very high optical isolation ( $> 30$  dB; e.g., 50 dB for an air-to-air surveillance radar) fiber-optic switch. Note that these stringent optical switch requirements arise because of the N-bit cascaded nature of the delay line, with N being as large as 13 bits. Micromechanics appears to be a promising fiber-optic switch technology for this high signal-to-noise ratio phased array application as micromachining could allow low cost, large volume batch fabrication of compact, low power, high optical isolation switches. Recent experimental results from electrostatic micromechanical optical switches have been promising; for example,  $> 40$  dB optical isolation and 3.1 dB insertion loss from a NTT 2 X 2 switch [3]. Note that switch cost is also a critical issue as typical large high performance phased array radars might have 10,000 antenna elements, and for 11-bit, element level control, 100,000 2 X 2 optical switches would be required for the system. Also note that cost and isolation/loss are key issues, and switching speeds of a millisecond can be tolerated if the novel time-multiplexed antenna scanning technique using two independent channels per antenna element is used for time delay control [1, 5-7]. For high temperature applications, e.g., 400 degrees Centigrade (C), in aircraft sensor networks, the micromechanical optical switch must withstand the harsh temperature environment.

#### 4. THE MEANDER-LINE GEOMETRY PIEZOELECTRIC THIN FILM ACTUATOR

The basic switch design uses a silicon substrate to provide the building block for the necessary fiber-optics, microoptics, and micromechanics that form the microdynamical fiber-optic switch architecture. The microactuators to be used are based on the meander-line geometry piezoelectric thin film actuators that have been recently demonstrated at the University of Minnesota [8-10]. Because the meander-line microactuator consists of two top electrodes and one bottom electrode, two basic modes of operation/actuators are possible. One actuator uses a folded path or meander line geometry (see Fig.4) to produce horizontal tethered (displacement about a fixed point) linear displacements. Another unimorph based vertical displacement actuator uses a ladder like geometry (see Fig.5), where a number of unimorph bars arranged in a planar format and connected in series mechanically produces a tethered displacement perpendicular to the plane containing the unimorphs. Thus, depending on the microactuator used, it is possible to generate either vertical or horizontal linear displacements.

The first mode of operation/actuator is based on piezoelectric extensions taking place parallel to the substrate (see Fig.4). A linear motion piezoelectric actuator having a compact design and large displacement capabilities has been theoretically designed and constructed on a macro-scale [7]. The prototype macro-scale actuator (see Fig.6) is composed of a number of parallel bars of PZT which are connected together in a meander line configuration so that they are mechanically in series and electrically in parallel. The piezoelectric polarity of the adjacent bars is arranged so that if a given bar expands under an applied voltage, the adjacent bars will contract when the same voltage is applied to every bar. Each bar is connected to the same power supply so that all of the bars are connected in parallel. Both ends of the meander line are clamped and the center of the meander line is the output where external loads are connected and where displacement relative to the clamped ends occurs. The center portion of the positioner is free to move and therefore because of the mechanical series connection of the bars, the changes in the length of each bar add together producing a net horizontal displacement. The absolute displacement of the output end of the meander line is the same as that of a single straight bar of the piezoelectric whose length is one half of the unwrapped meander line assuming equivalent applied voltages. Note that for the thin film microactuator, the piezoelectric polarity reversal is achieved by using dual electrodes deposited on the PZT film corresponding to each bar, with one wide electrode and one very thin electrode, and using positive and negative drive voltages for displacement control. Here, the lower surface of all the thin-film bars acts as the ground electrode. Note that the maximum temperature at which the piezoelectric actuator can operate is a function of the material which comprises the unimorphs; for example, aluminium nitride can operate in temperatures up to about 700 degrees C, zinc oxide up to about 500 degrees C, lead zirconate titanate (PZT) up to about 380-400 degrees C, and lead titanate up to about 340 degrees C.

The prototype actuator studied made use of 22 bars of PZT, each 4 cm long, 3 mm wide, and 1.5 mm thick. The measured displacement for an applied dc voltage of 500 V (electric field of approximately 3 kV/cm) was 45  $\mu$ m. A plot of the unloaded actuator displacement versus applied voltage is shown in Fig.7. The measured force output at 500 V was 0.3 N. Two stiffeners were added to the basic structure as illustrated in Fig.8 which increased the force output by a factor of three without affecting the displacement capabilities of the actuator. The displacements and forces measured are in agreement with the predictions of a theoretical electromechanical model of the actuator [11].

The important implications of the macromodel work has lead to scaled-down performance calculations for a microscale horizontal positioning device. A representative design simulation shows the performance of PZT,  $\text{PbTiO}_3$ , and  $\text{ZnO}$  piezoelectric materials. As shown in Fig.9, a 20 V differential potential applied to the PZT device structure produces a 10  $\mu\text{m}$  horizontal displacement for a structure consisting of 20 piezoelectric bars. Note that as compared to electrostatic-based actuators, these piezoelectric thin film based actuators can give the desired (e.g., 10  $\mu\text{m}$ ) displacements in a few tens of volts instead of a hundred or more volts. A calculation of generated force and displacement versus bar width (bar length is fixed at 500  $\mu\text{m}$ ) has been carried out in Fig. 10. While this figure exhibits a classical trade-off between force and displacement, the very large force generation capability gives this device the potential for higher speed switching.

The other kind of actuator is the vertical displacement microactuator that uses a trellis-like geometry shown in Fig.5. The trellis is constructed of multilayer bars composed of a mechanical structural support base layer, PZT thin film, and a dual top electrode structure. The piezoelectric material is asymmetrically located with respect to the longitudinal neutral axis of the bar which results in a so-called unimorph structure. When voltages are applied to the dual electrodes as indicated in Fig.5, bending moments are generated about the longitudinal neutral axis of each element. The voltage polarity of the wide electrode (the polysilicon or tungsten layer is ground) on the top surface of each element governs whether the piezoelectric film expands or contracts. If the piezoelectric film expands, the unimorph element bends concave up, as indicated on the diagram of a single unimorph structure shown in Fig.11. Contraction of the piezoelectric film bends the unimorph element concave down. A given electrode alternates from being wide on one element to being narrow on the adjacent two elements and this in turn causes adjacent unimorph elements to bend in opposite directions as indicated in Fig.11. The theoretical operation and experimental verification of this device has been carried out on a macroscale [10,12]. Fig. 12 shows representative simulated results expected in the microfabricated device. The relatively large displacement and forces associated with this structure are promising for switching applications where larger microoptics is needed in coupling in and out of fibers, such as when using GRIN rod lenses.

## 5. FABRICATION

A fabrication process for a micromechanical version of the meander-line mirror has been developed for both  $\text{ZnO}$  and PZT based devices. The basic fabrication sequence for the PZT device is on a silicon substrate and is diagrammed in Fig.13. Device fabrication is based on ferroelectric surface-micromachining techniques which have been developed at the University of Minnesota over the last two years [12]. Fabrication begins with a suitable starting substrate. The substrate can be either silicon or gallium arsenide but is typically covered with a stress-relief layer of silicon dioxide and a chemical protection barrier of silicon nitride. These wafers may or may not contain integrated circuits. For the positioning of optical fibers, a V-groove is first etched into the silicon wafer by anisotropic etching. The etching depth is tailored to orient the centers of the optical fibers with the center of the movable tungsten mirror that is part of the mechanical structure that forms the thin-film microactuator. The preliminary design described below does not include silicon-based microoptics such as focussing lenses that might be required if the mirror thickness or height is not adequately large to prevent substantial light loss. Under certain design conditions, the optical loss can be minimized without using focussing optics.

The basic fabrication for PZT devices fabricated on silicon substrates is described as follows. In Fig. 13.1, a 0.7-1.0  $\mu\text{m}$ -thick sacrificial layer of phosphosilicate glass (PSG) is deposited by low pressure chemical vapor deposited (LPCVD) onto the silicon nitride covered silicon substrate (not shown) and patterned. A 5.0-10  $\mu\text{m}$ -thick film of tungsten is then deposited and patterned (Fig. 13.2). Tungsten serves as the micromechanical support layer with double attachment points to the silicon nitride covered substrate. Our recent work on piezoelectric pressure sensors [13] confirms its inherent strength as a micromechanical material [14]. It has the additional advantage that it does not require the high temperature (1050  $^{\circ}\text{C}$ ) stress-relief anneal step required for polysilicon micromechanical structures [15-16]. The tungsten film is patterned using dry etching techniques. This leads to a nearly vertical end necessary for the optical mirror to reflect in the plane of the incident light. A thin layer of titanium 500  $\text{\AA}$  is then deposited by sputtering to form an adhesion layer for the subsequently deposited PZT thin films (Fig. 13.3). Sol-gel deposited PZT is then spun in successive 800-900  $\text{\AA}$  coatings over the wafer. A typical final PZT thickness is 0.6  $\mu\text{m}$ . Our PZT processing details are more fully described in Ref. [17]. Crystalline firing is carried out at 650  $^{\circ}\text{C}$ . The PZT film is then patterned using sputter etching or ion assisted etching [18] leaving the structure shown in Fig.13.4. Metal electrodes are then formed over the surface of the micro-meander line as shown in Fig.13.5. These electrodes are formed by the sequential deposition of tungsten and aluminum. The tungsten is necessary for making a good electrical contact to the top of the PZT layer. The aluminum is needed for making electrical contact to the

two metal lines on the top of the meanderline and the bottom electrode. A final photolithography step is then used to protect the top PZT layer and electrodes. Because the PSG layer is designed to slightly protrude from underneath the tungsten meander line, open regions in the photoresist allow undercutting of the meander line to take place. The PSG layer etches rapidly in the hydrofluoric acid. The PSG is etched both vertically and laterally in this surface-micromachining step. Single mode optical fibers are then manually inserted in the V-groove trenches. This completes the device processing. Note that it is also possible to replace the fibers with glass optical waveguides that are fabricated with the rest of the microactuator.

A fabrication run using ZnO thin films ( $d_{31} = 6 \text{ pC/N}$ ) was completed and observable movement of approximately  $2.3 \mu\text{m}$  was noted for a device with sixteen bars measuring  $80 \times 500 \mu\text{m}^2$  with 80 V differential actuation applied to the top electrodes. We anticipate better performance with a PZT-based structure due to the substantially higher piezoelectric coefficient ( $d_{31} = 280 \text{ pC/N}$ ). We have had some success in addressing some of the important issues for piezoelectric MEMS. We have already demonstrated the capability to fabricate some ferroelectric thin-film-based microsensors using sol-gel fabrication procedures [19-20] and surface-micromachined tungsten structures [13]. Integration of such sensors with signal-level CMOS circuitry has also been demonstrated in the form of a fully functional  $64 \times 64$  element  $\text{PbTiO}_3$  pyroelectric imaging array with over 10,000 MOS transistors [21]. Several PZT-based actuator concepts including linear stepper motors [22] have been proposed, and microscale versions of these actuators have been designed and fabrication efforts are beginning.

## 6. FIBER-OPTIC SWITCH DESIGN

As shown in Fig.13.6, part of the mechanical structure that forms the microactuator is also the tungsten mirror that on translation implements the optical switching operation. The actual thickness (or height) of this mirror is critical to the design of a low loss optical switch. A typical thickness of the tungsten layer is between 5-10  $\mu\text{m}$ . This means that the optical beam illuminating the tungsten surface be less than 10  $\mu\text{m}$  in diameter. This condition can be satisfied in two ways.

One way is to use single mode fibers with mode field diameters that are less than 10  $\mu\text{m}$ , with the inter-fiber distance between input and output fibers of less than 50  $\mu\text{m}$ . The fibers must have small numerical apertures, e.g., 0.11. This arrangement of fibers prevents excessive optical loss as the light out of the fiber is in its near-field propagation path, and has not spread greatly so as to be only partially reflected by the tungsten mirror. A typical single mode fiber has a core diameter of 3.2  $\mu\text{m}$  at 514 nm and a numerical aperture of 0.11, with a mode field width of 3.7  $\mu\text{m}$ . Note that the single-mode optical fibers are arranged in a fixed geometry, held in the silicon V-grooves that have been precision etched within sub-micron tolerances. Fig.14 and Fig.15 show the basic optical architectures for a  $1 \times 2$  and  $2 \times 2$  micromechanical fiber-optic switch, respectively. Note that the angle between the incident optical beam and reflected optical beam are designed such as to minimize Fresnel transmission and reflection optical losses [3].

The second way to design the optical fiber switch is to use small imaging lenses to focus the light emanating from a fiber onto the mirror surface (see Fig.16). In this way, the light from the fiber strikes the tungsten film as a narrow focussed spot of < 10  $\mu\text{m}$  diameter. Note that this approach forces the inter-fiber input-output distance to be several millimeters instead of a few tens of microns. This is because the fiber lenses are 1-2 mm in diameter with a few millimeter focal lengths. These fiber lenses can be GRIN-type imaging lenses or silica glass lenses fabricated on the silicon optical bench that contains the silicon V-grooves for the fibers. Fig.14-15 depict switch designs that requires horizontal linear translations to implement the switching operation. Note that a vertical displacement actuator can also be used to do the optical switching where the thin-film actuator-based mirror is lifted for switching.

## 7. THE OPTICAL EXPERIMENT TO TEST ACTUATOR STABILITY

Fig.17 shows a photograph of the PZT macroactuator formed using 22 PZT bars, with a bar size of 4 cm length, 3 mm width, and 1.5 mm thickness. The Figure also shows the 2.5 cm diameter mirror attached to the center of the macroactuator. Fig.18 shows the optical test bed for high accuracy displacement measurements and macroactuator stability verification. The optical set-up is a Michelson interferometer, with the macroactuator mirror placed in one arm of the interferometer. The output of the optical system is a fixed fringe pattern, as shown in the CCD output of Fig.19. A photo-diode is placed at a fixed position in the output fringe pattern. When the macroactuator mirror moves in a linear horizontal fashion on applying a voltage to the PZT macroactuator, the fringe pattern shifts causing the signal output from the photo-diode to show a sinusoidal behavior. Note that the optical fringe shifts one

cycle when the light undergoes a one optical wavelength phase shift. Because the light from the macroactuator mirror retraces its path on reflection, a half wavelength motion of the mirror causes a one cycle shift in the fringe pattern. Thus, since we are using 632 nm wavelength light, a 316 nm motion of the mirror corresponds to one cycle in the photodiode output. Fig.20 shows the data output from the photo-diode for a changing macroactuator applied voltage, while Fig.21 shows the actual loaded displacement suffered by the macroactuator mirror. These experiments provide a displacement resolution of < 100 nm. Moreover, the presence of a stable fringe pattern for a given applied voltage (as seen in Fig.19) indicates that the macroactuator operation is stable to within a few tens of nanometers. This shows the rather exceptional stability of the macroactuator; a condition required when using the microactuator with single mode fiber-optics.

## **8. CONCLUSION**

This paper has introduced the use of micromachined piezoelectric thin-film microactuators for applications in fiber-optic switching. Test models of the thin-film microactuators have been built and tested. Recently, a microscale device using PZT was fabricated and tested. Fig.22 shows the device and performance graph indicating approximately 4.1  $\mu\text{m}$  displacement for a 80 V differential actuation. Better results are expected with improved fabrication runs. Next, research into the optical components of the switch are underway. In particular, issues such as low loss input-output fiber coupling are being analyzed, along with options for microoptics (such as GRIN lenses) for efficient, low loss optical switching.

## **9. ACKNOWLEDGEMENTS**

Support from GECRD is greatly appreciated. Thanks to John Herkert for making the optical measurements. The work at the University of Minnesota is supported by the National Science Foundation.

## **10. REFERENCES**

- [1] N. A. Riza, "Liquid crystal-based optical time delay control system for wideband phased arrays," *Analog Photonics OE/Fibers Conference Proceedings of the International Society of Optical Engineering (SPIE)*, Vol. 1790-23, Sept., 1992.
- [2] K. Hogari and T. Matsumoto, "Electrostatically driven fiber-optic micromechanical on/off switch and its applications to subscriber transmission systems," *IEEE Journal of Lightwave Technology*, Vol. 8, No.5, May 1990.
- [3] K. Hogari and T. Matsumoto, "Electrostatically driven micromechanical 2  $\times$  2 optical switch," *Applied Optics*, Vol. 30, No. 10, pp. 1253-1257, 1991.
- [4] G. A. Magel and J. L. Leonard, "Phosphosilicate glass waveguides for phased array radar time delay," *SPIE Proc.* 1703-48, 1992
- [5] N. A. Riza, "A compact high performance optical control system for phased array radars," *Inst. of Electrical and Electronic Engineers (IEEE) Photonics Tech. Lett.*, Vol.4, No.9, pp.1073-1076, Sept., 1992.
- [6] N. A. Riza, "Phased array antenna control using liquid crystals," *Analog Photonics OE/Fibers Conference Proceedings of the International Society of Optical Engineering (SPIE)*, Vol. 1790-08, Sept., 1992.
- [7] N. A. Riza, "Liquid crystal-based optical control of phased array antennas," *Inst. of Electrical and Electronic Engineers (IEEE) and Optical Society of America (OSA) Journal of Lightwave Tech.*, Dec., 1992.
- [8] W. P. Robbins, D. L. Polla, and D. E. Glumac, "High-Displacement Piezoelectric Actuator Utilizing a Meander-Line Geometry- Part I: Experimental Characterization," *IEEE Trans. Ultrasonics, Ferroelectrics, and Frequency Control*, Vol. 38, No. 5, Sept. 1991.
- [9] W. P. Robbins, D. L. Polla, and D. E. Glumac, "A planar unimorph-based actuator with large vertical displacement capability," *Journal of Micro-Engineering*, Vol.1, 1991.
- [10] W. P. Robbins, D. L. Polla, T. Tamagawa, D. E. Glumac, and J. W. Judy, "Linear Motion Microactuators Using Piezoelectric Thin Films," 6th Int. Conference on Sensors and Actuators (Transducers '91), San Francisco, CA, 1991. "Design of Linear Motion Microactuators Using Piezoelectric Thin Films," *J. of Micromechanics and Microengineering*, (1991).
- [11] W. P. Robbins "High Displacement Piezoelectric Actuator Utilizing a Meander Line Geometry - Part II: Theory," *IEEE Trans. on Ultrasonics, Ferroelectrics, and Freq. Control*, 38, p. 454, (1991).
- [12] T. Tamagawa, D.L. Polla, and C.-C. Hsueh, "Lead Zirconate Titanate (PZT) Thin Films in Surface-Micromachined Sensor Structures," *IEEE International Electron Devices Meeting*, San Francisco, Dec. 1990.

- [13] P. Schiller, "Surface-Micromachined Piezoelectric Pressure Sensors," M.S. Thesis, University of Minnesota, December 1991.
- [14] L. Y. Chen, Z. L. Zhang, J. J. Yao, D. C. Thomas, and N. C. MacDonald, "Selective Chemical Vapor Deposition of Tungsten for Microdynamic Structures," *Proc. IEEE Micro Electro Mechanical Systems*, Salt Lake City, Utah, p. 82, 1989.
- [15] H. Guckel, J. J. Sniegowski, and T. R. Christenson, "Advances in Processing Techniques for Silicon Micromechanical Devices with Smooth Surfaces," *Proc. IEEE Micro Electro Mechanical Systems*, Salt Lake City, Utah, p. 71, 1989.
- [16] R. T. Howe, "Surface Micromachining for Microsensors and Microactuators," *J. Vac. Sci. and Technol. B*, 6, 1809 (1990).
- [17] C.-C. Hsueh, T. Tamagawa, C. Ye, A. Helgeson, and D. L. Polla, "Sol-gel Derived Lead Zirconate Titanate (PZT) Films," *3rd International Symp. on Integrated Ferroelectrics*, Colorado Springs, CO, Mar. 1991. *Ferroelectrics*, 1992.
- [18] P. F. Baude, C. Ye, T. Tamagawa, and D. L. Polla, "Fabrication of Sol-Gel Derived PLZT (9/65/35) Optical Waveguides," *Mat. Res. Soc. 1991 Fall Meeting*, Boston, MA, Dec. 1991.
- [19] D. L. Polla, C. Ye, and T. Tamagawa, "Surface-Micromachining of PbTiO<sub>3</sub> Pyroelectric Detectors," *Appl. Phys. Lett.* 59, 3539, (1991)
- [20] C. Ye, T. Tamagawa, Y. Lin, and D. L. Polla, "Pyroelectric Microsensors by Sol-Gel Derived PbTiO<sub>3</sub> and La-PbTiO<sub>3</sub> Thin Films," *Mat. Res. Soc. 1991 Fall Meeting*, Boston, MA, Dec. 1991.
- [21] L. Pham and D. L. Polla, "Surface-Micromachined Three-Dimensional Integrated Sensors," *IEEE J. of Solid State Circuits*, 1991.
- [22] J. Judy, D. L. Polla, and W. P. Robbins, "A Linear Piezoelectric Stepper Motor with Sub-Micrometer Displacement and Centimeter Travel," *IEEE Trans. on Ultrasonics, Ferroelectrics, and Frequency Control*, UFFC-37, 428-437, 1990.



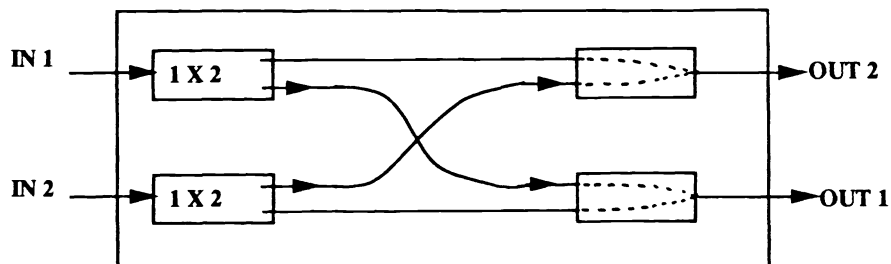
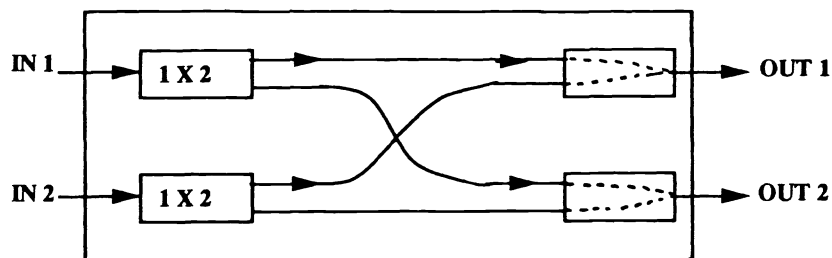
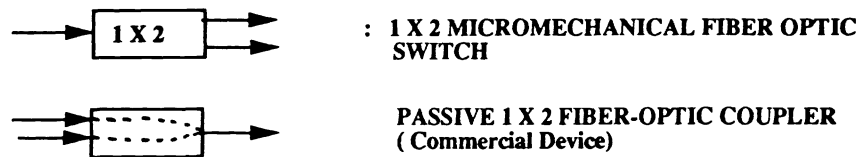


Fig.1. The 1 X 2 optical switch configuration using two standard passive fiber-optic couplers to give a 2 X 2 configuration.

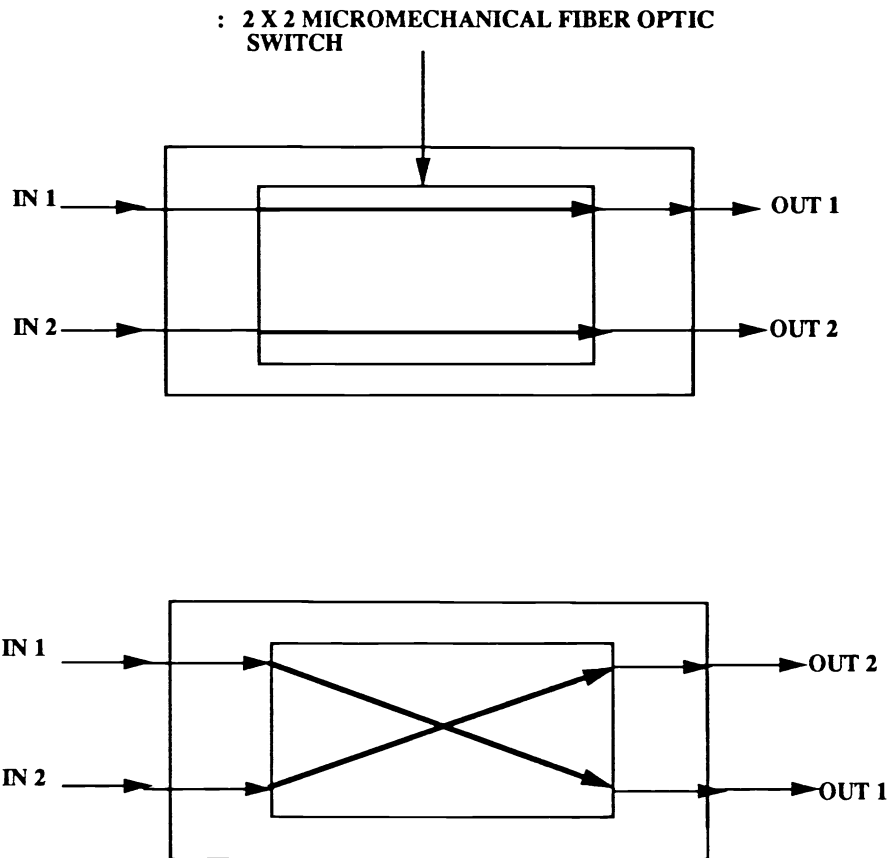


Fig.2 The 2 X 2 optical switch configuration.

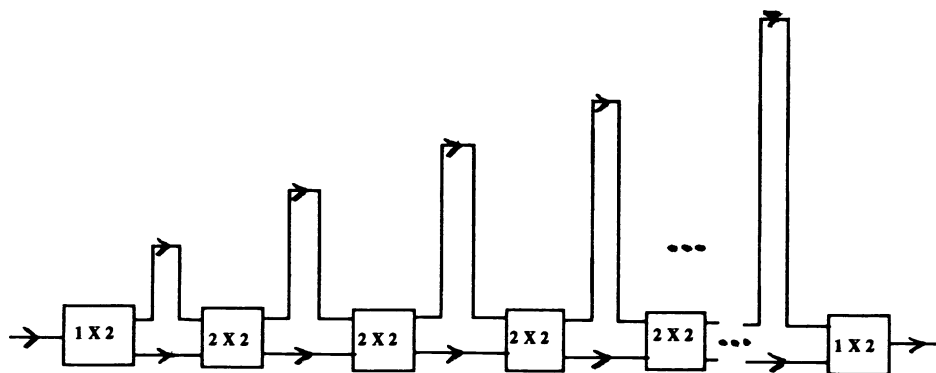


Fig.3 shows a typical serial digitally switched delay line structure that is required for controlling an antenna element or subarray in a wide bandwidth phased array radar.

# PIEZOELECTRIC LINEAR MICROACTUATOR

## Meanderline Actuator based on ZnO and PZT Thin Films

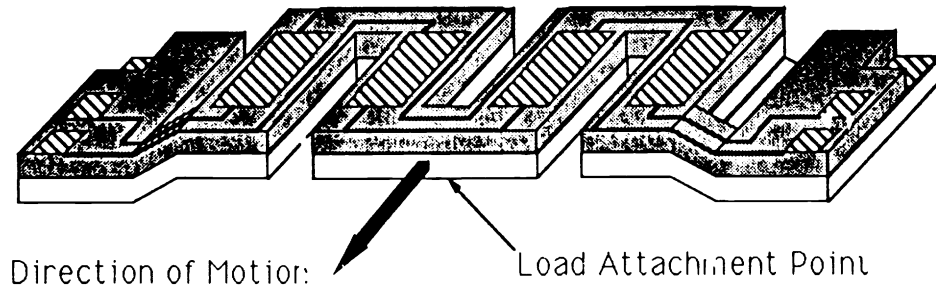


Fig.4 The meander-line geometry piezoelectric thin film microactuator.

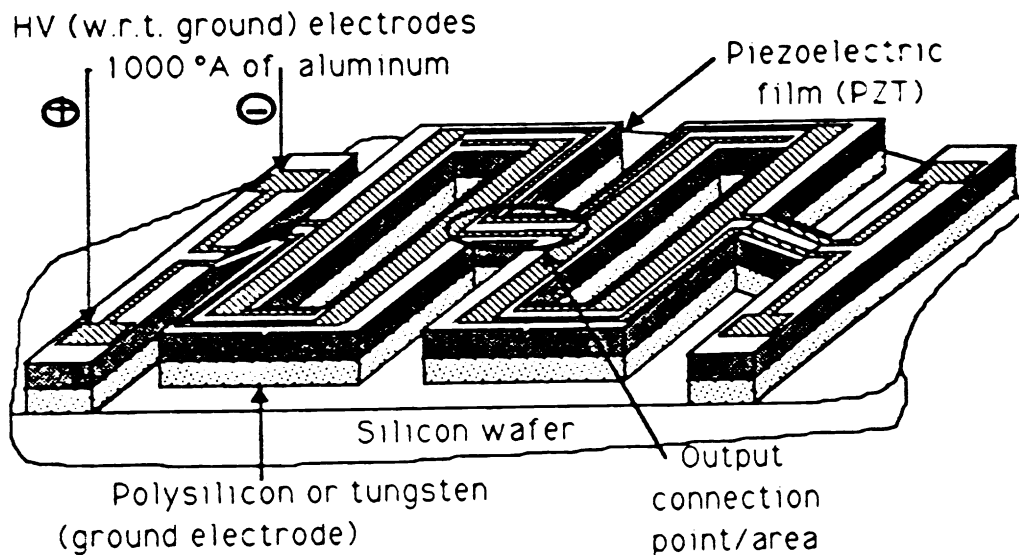


Fig.5 Unimorph based vertical displacement thin-film microactuator using a ladder like geometry.

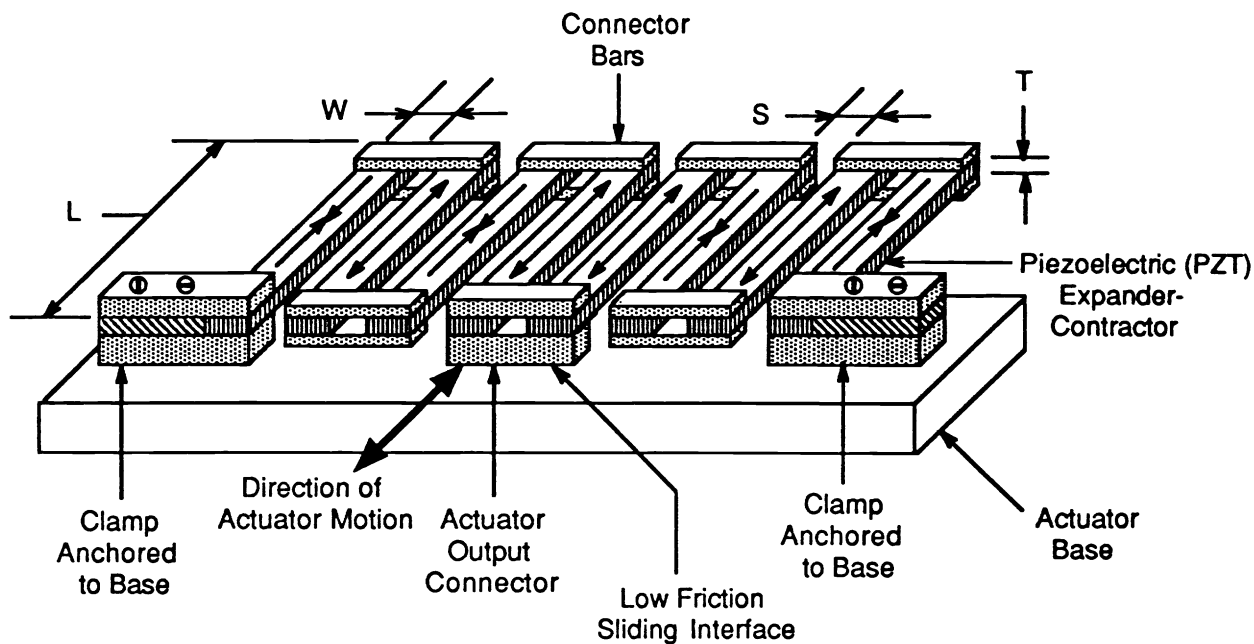


Fig.6 Prototype macroscale meander-line actuator for producing linear displacements.

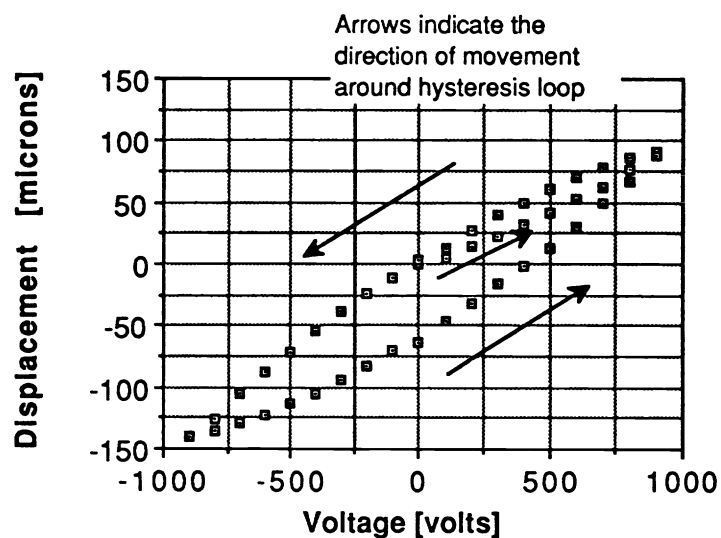


Fig.7 Meander-line actuator output displacement as a function of applied voltage with no applied load.

Stiffeners

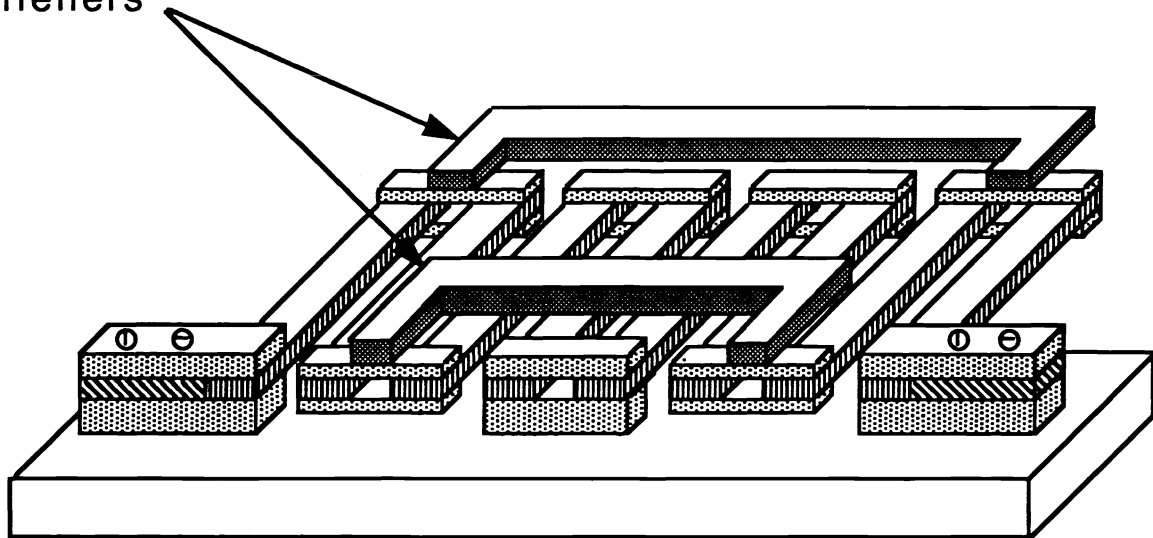


Fig. 8. Application of stiffeners to increase the force output of the meander-line actuator without affecting the displacement versus voltage characteristic.

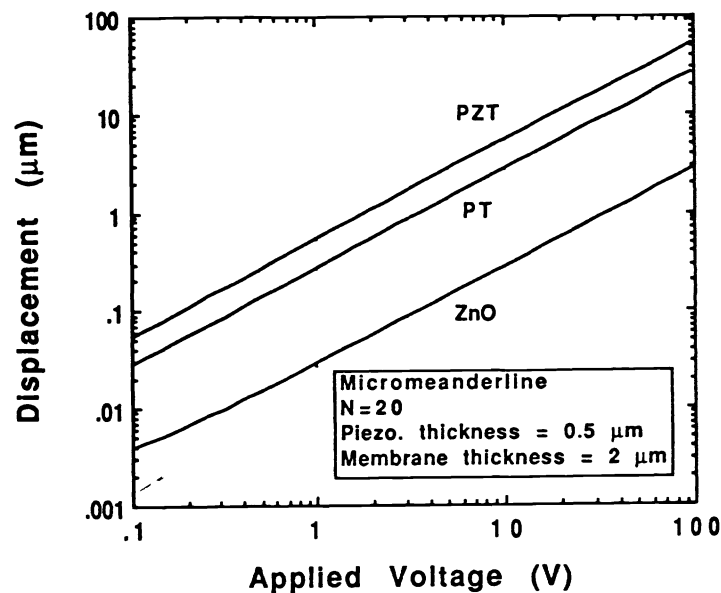


Fig.9 shows that a 20 V differential potential applied to the PZT device structure produces a  $10 \mu\text{m}$  horizontal displacement for a structure consisting of 20 piezoelectric bars. Typical meander-line geometries within the capabilities of fabrication technology have been assumed.

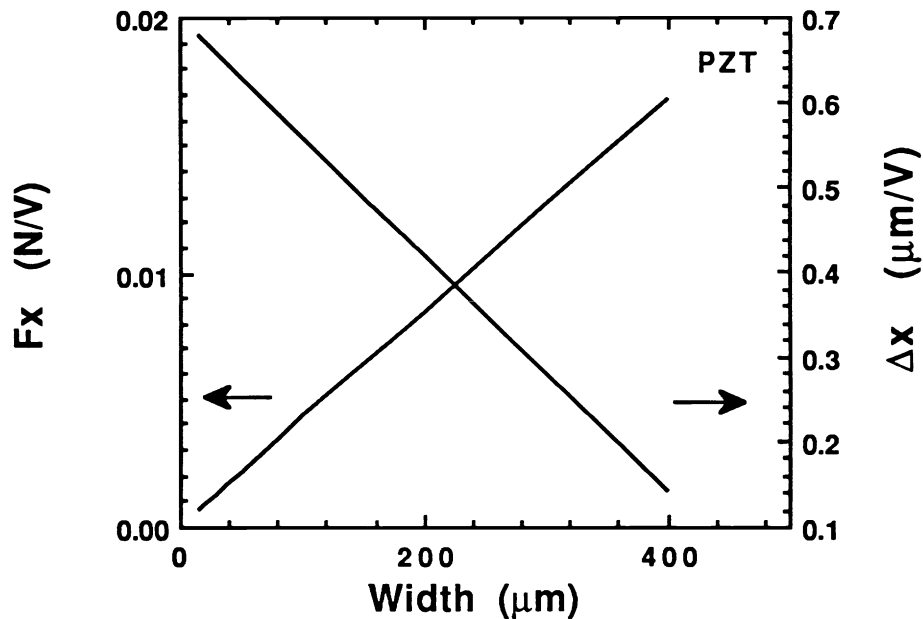


Fig. 10 shows a calculation of generated force and displacement versus bar width (bar length is fixed at 500  $\mu\text{m}$  and PZT thickness is 0.5  $\mu\text{m}$  ).

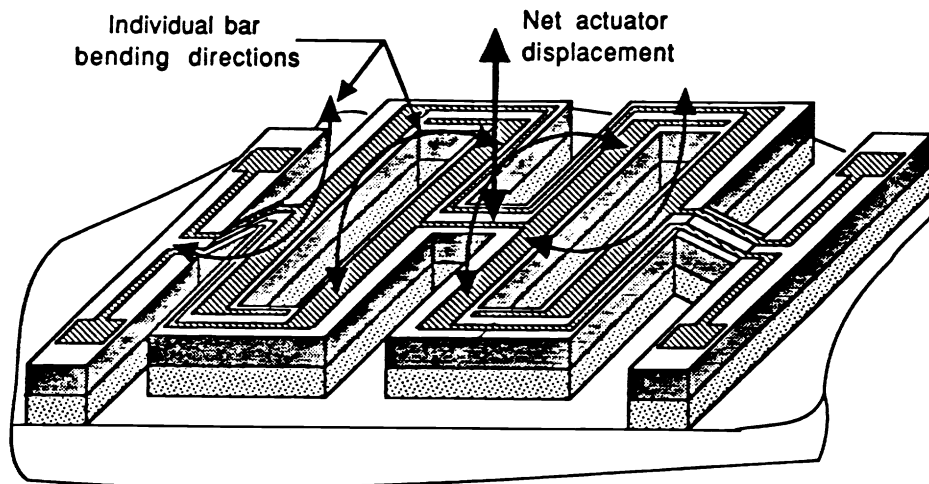


Fig.11 Perspective view of unimorph-based microactuator showing bending of each bar and how individual vertical displacements of each bar add up to produce the total actuator output.

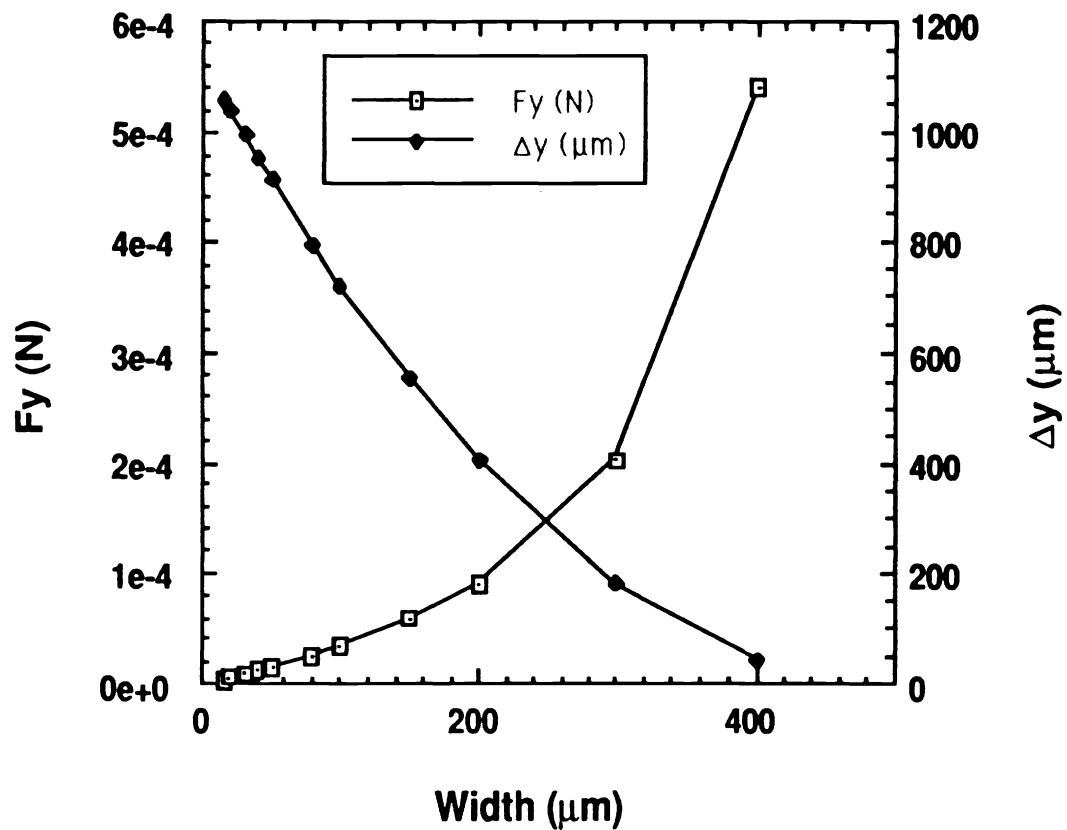


Fig.12 Calculated vertical displacement and force for a vertical microactuator structure using 500 long PZT bars with a thickness of 0.5. Other typical material parameters and reasonable dimensions have been assumed.

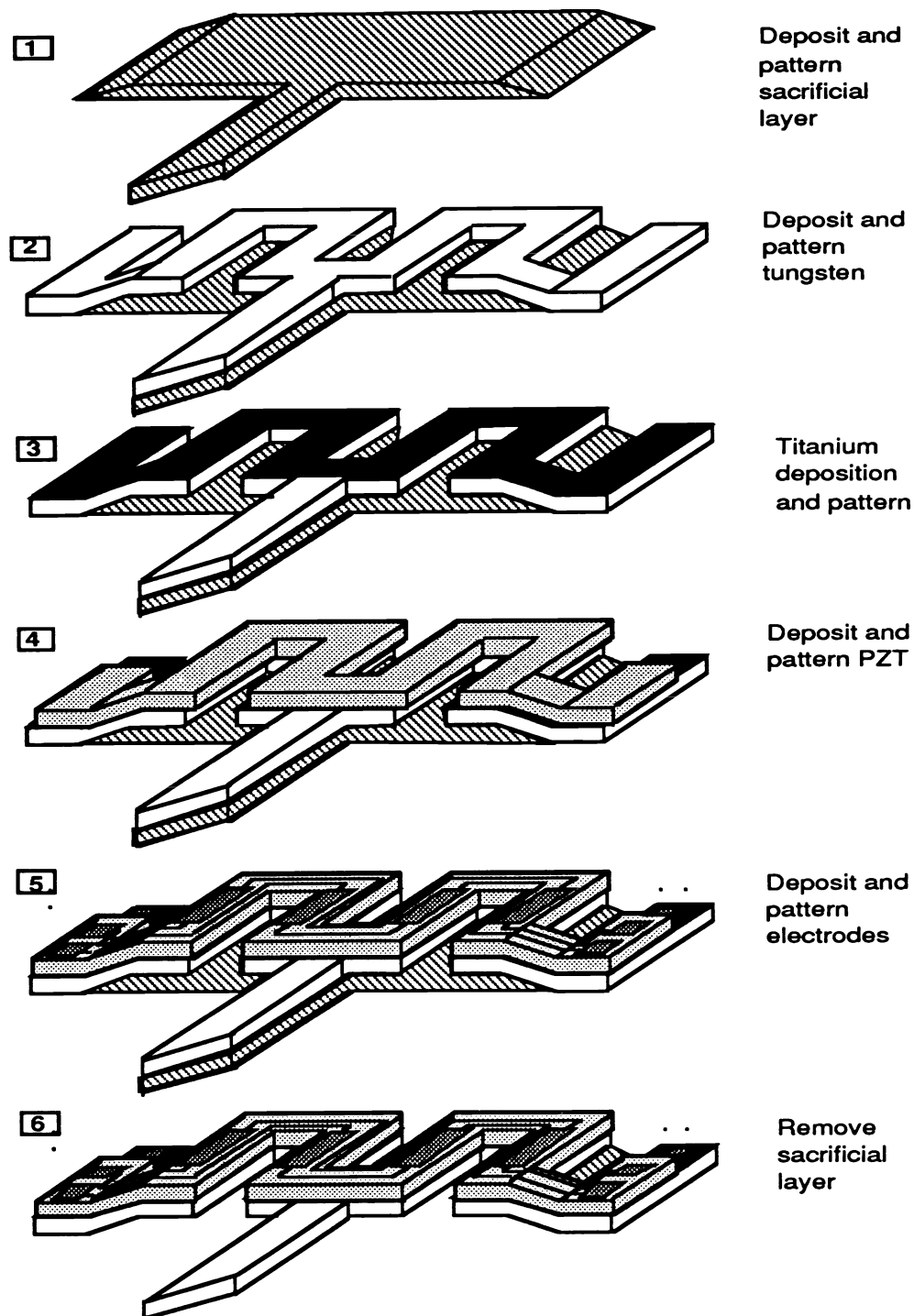


Fig. 13. Basic fabrication sequence for the horizontal PZT micromechanical fiber-optic switch.



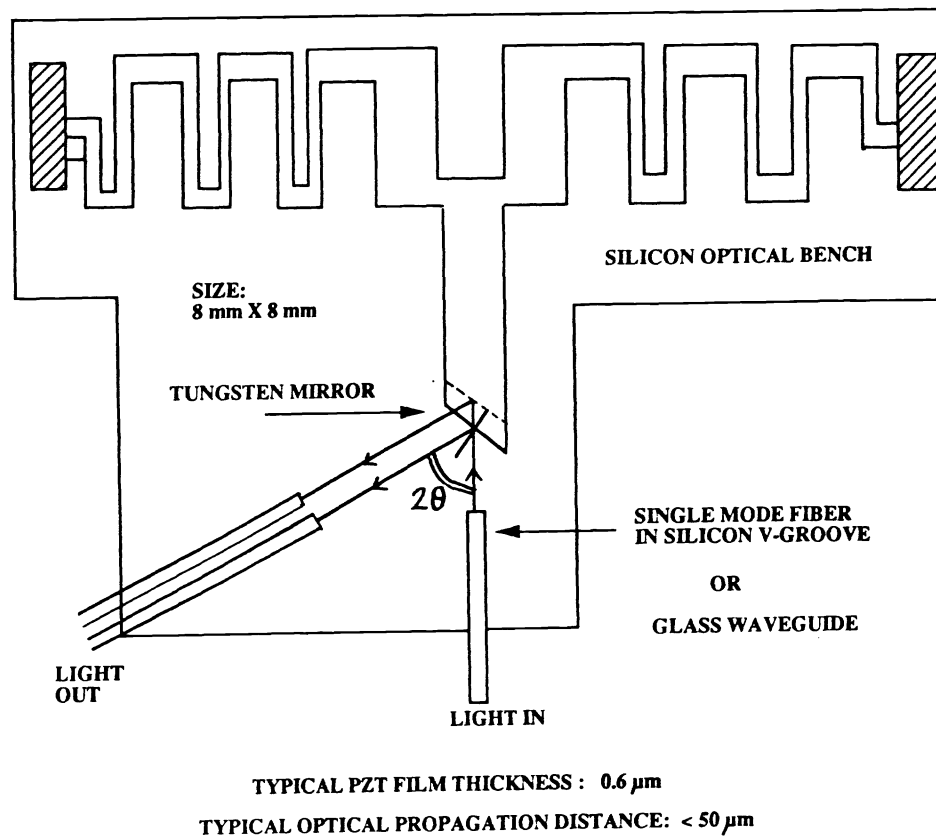


Fig.14 The 1 X 2 micromechanical optical switch design configuration using the horizontal displacement piezoelectric thin-film microactuator.

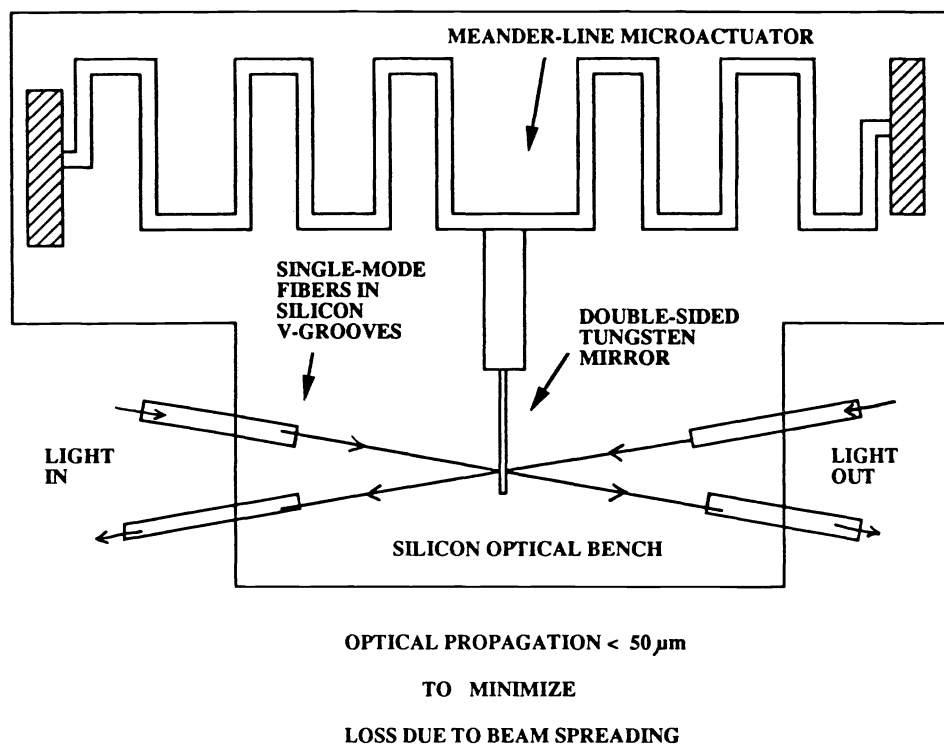


Fig.15 The 2 X 2 micromechanical optical switch design configuration using the horizontal displacement piezoelectric thin-film microactuator.

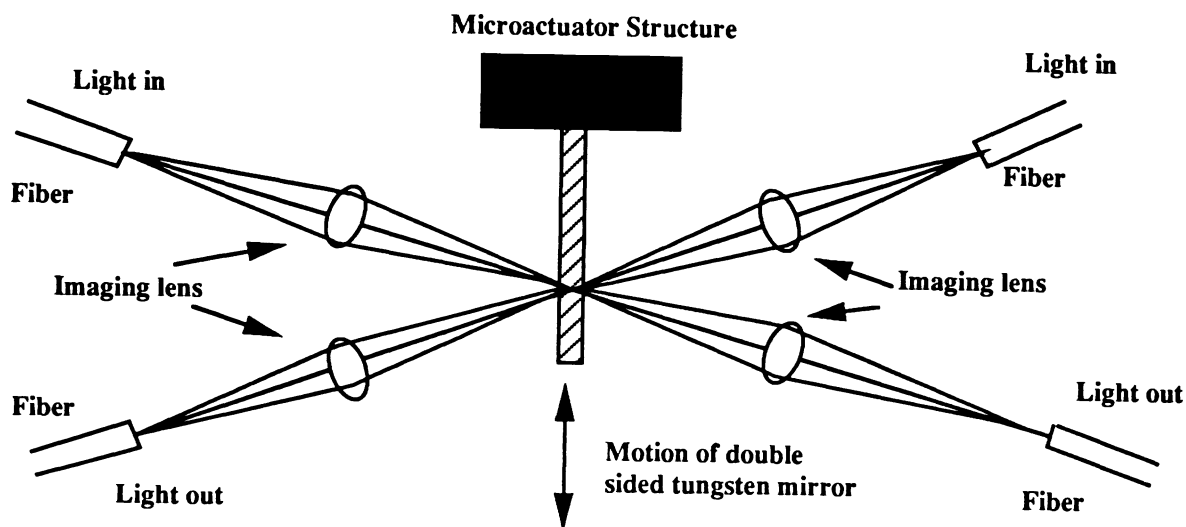
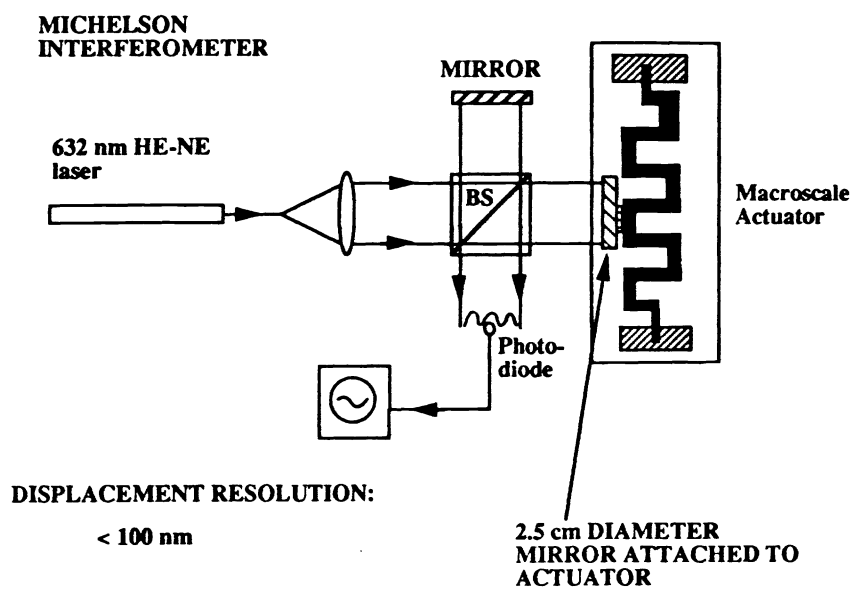


Fig.16 The 2 X 2 micromechanical optical switch configuration using microoptic fiber imaging lenses.



**Fig.17 Photograph of macroscale meander-line actuator with mirror mounting.**



**Fig.18 shows the optical test bed for high accuracy displacement measurements and macroactuator stability verification.**



Fig.19 CCD camera output showing fringe pattern at the output of the michelson interferometer that contains the macroactuator mirror.

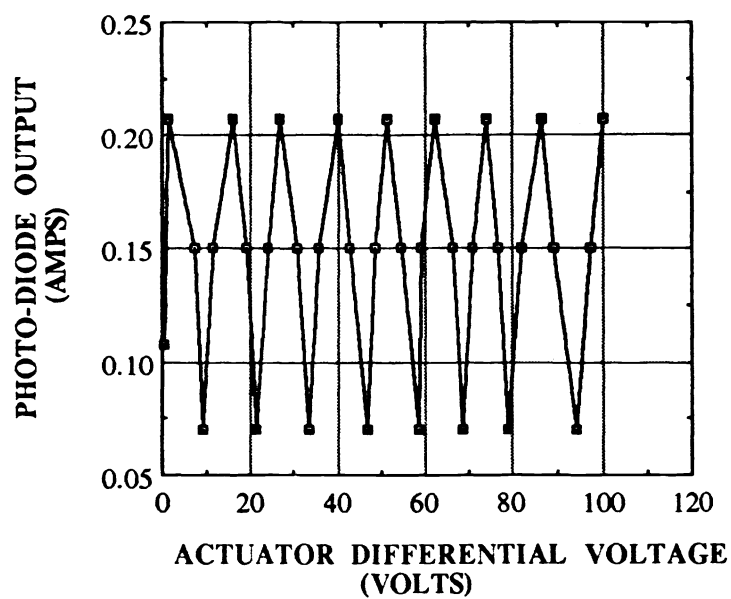


Fig.20 Photodiode current output for a changing macroactuator applied voltage.

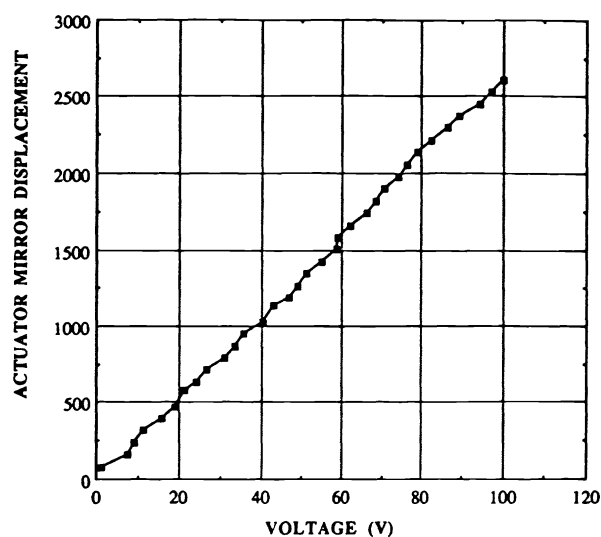


Fig.21 Plot of macroactuator mirror motion response to a changing applied voltage.

## Micromechanical Piezoelectric Positioner

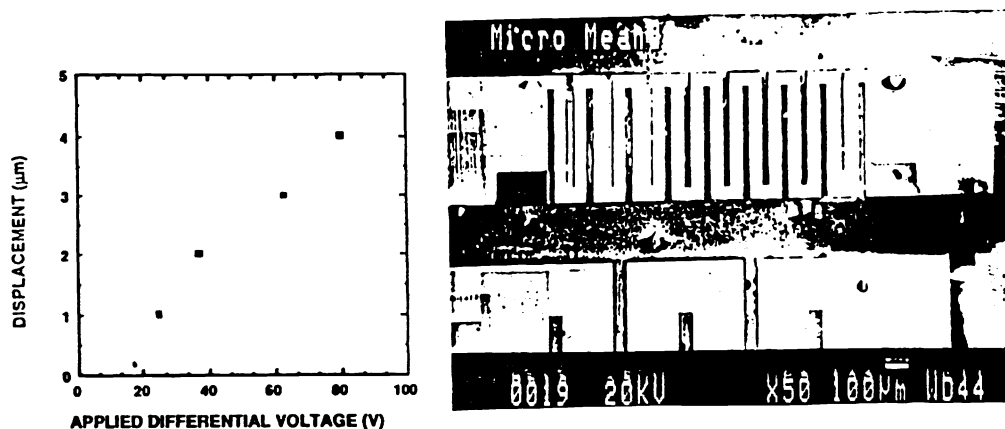


Fig.22 shows the recently fabricated microscale device using PZT. The Figure also shows the performance graph indicating approximately  $4.1 \mu\text{m}$  displacement for a 80 V differential actuation.